Research Article

Structural, Nanomechanical, and Field Emission Properties of Amorphous Carbon Films Having Embedded Nanocrystallites Deposited by Filtered Anodic Jet Carbon Arc Technique

R. K. Tripathi, O. S. Panwar, A. K. Srivastava, Ishpal, Mahesh Kumar, and Sreekumar Chockalingam

Polymorphic Carbon Thin Films Group, Physics of Energy Harvesting Division, CSIR-National Physical Laboratory, Dr. K. S. Krishnan Road, New Delhi 110012, India

Correspondence should be addressed to O. S. Panwar; ospanwar@mail.nplindia.ernet.in

This paper reports the effect of substrate bias on the structural, nanomechanical, and field emission properties of amorphous carbon films having embedded nanocrystallites (a-C:nc films) deposited by filtered anodic jet carbon arc technique. X-ray diffraction results exhibit predominantly an amorphous nature of the films. High-resolution transmission electron microscope images showed the amorphous nature of the films with nanocrystallites embedded in the amorphous matrix. Ultrafine nanograined microstructures with average grain size between 20 and 30 nm are observed throughout the film with a majority of the grains of single crystallites. A strong influence of substrate bias has been observed on the structural, nanomechanical, and field emission properties. Maximum nanohardness (H) of 58.3 GPa, elastic modulus (E) of 426.2 GPa, and H/E of 0.136 have been observed in a-C:nc films deposited at -60 V substrate bias which showed 82.6% sp^3 content.

1. Introduction

Amorphous carbon films have been center of attention for a variety of applications due to their chemical inertness, high optical transparency in the visible and near infrared, good adhesion to different substrates, low surface roughness, and good electrical, mechanical, and field emission properties [1–10]. The a-C films have been deposited by various techniques such as filtered cathodic vacuum arc (FCVA) [11–15], pulsed laser deposition (PLD) [16], sputtering, and electron cyclotron resonance (ECR) [17]. Compared to other deposition techniques, FCVA process offers the unique opportunity of growing different forms of carbon ranging from diamond-like to graphite-like and various intermediate materials such as tetrahedral amorphous carbon (ta-C), hydrogen and nitrogen incorporated ta-C (ta-C: H, ta-C: N), nanoclusters, nanocomposites, and nanotubes. The properties of carbon films mainly depend on the process parameters such as substrate bias, system geometry, pressure, arc current, and arc voltage and the environmental conditions during the growth of the films. There are established theoretical [18] and experimental [19] methods for the formation of different carbon nanostructures such as nanotube and fullerene by arc discharge. Amaratunga et al. [19–21] reported the deposition of hard and highly elastic carbon films which consist of graphitic sp^2 bonding using a graphite cathode with localized high pressure of helium or nitrogen at the arc spot. Depending upon whether the gas is injected through the cathode or anode, the technique will be termed as cathodic jet carbon arc (CJCA) or anodic jet carbon arc (AJCA). Alexandrou et al. [22, 23] have synthesized and characterized amorphous carbon films with embedded nanocrystallites deposited by unfiltered anodic jet carbon arc method with nitrogen gas. Chu and Li [24] have characterized amorphous and nanocrystalline carbon films. It is found that the properties of these carbon films were comparable to those of fullerene and carbon nanotubes [25, 26]. Lungu et al. [27] have reported carbon films containing nanodiamond crystallites embedded in a disordered graphite matrix deposited by the hydrogen-free thermionic vacuum arc method.
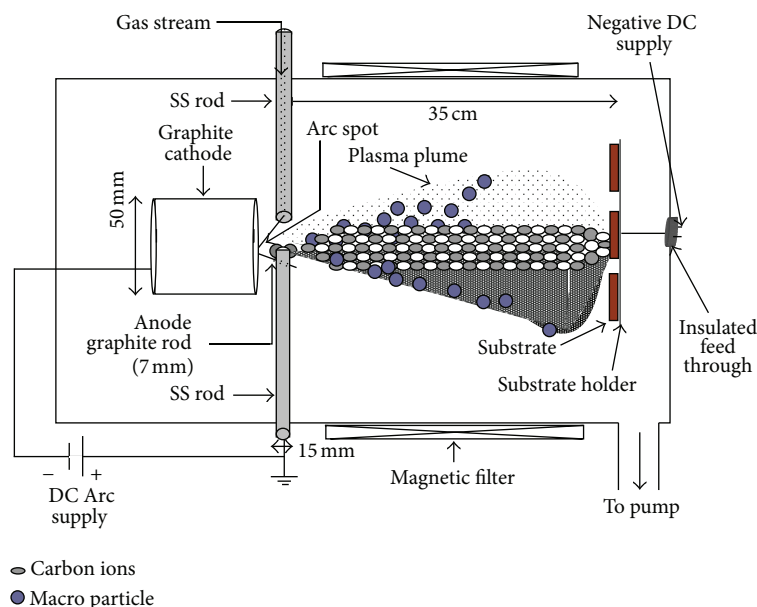
FIGURE 1: Schematic representation of filtered anodic jet carbon arc (FAJCA) technique for the deposition of a-C:nc films.

In the present technological trend, these carbon thin films having embedded nanocrystallites might be useful in producing mechanical devices with dimensions measured at micro/nanoscale. The ability of carbon to form different types of interatomic bonds to take different sites and to adopt different structures makes it a better material not only for nanomechanical devices but also for hard and protective coating on tools, solar cells, magnetic storage media, and automobile parts and field emission devices. Improved mechanical properties may play a vital role in many types of products.

The objective of this paper is to investigate the effect of negative substrate bias on the structural, nanomechanical, and field emission properties of amorphous carbon films having embedded nanocrystallites (a-C:nc) deposited using filtered anodic jet carbon arc (FAJCA) technique using helium gas. For comparison, we also refer to the properties of ta-C films deposited using an S bend FCVA process [12] and a-C films with embedded nanocrystallites deposited using filtered cathodic jet carbon arc (FCJCA) technique [28].

2. Experimental Details

2.1. Sample Preparation. Figure 1 shows the schematic representation of FAJCA technique used for the deposition of a-C:nc films. The FAJCA technique is based on striking the arc (arc voltage ~20–24 V with an arc current of ~56 A) between two graphite electrodes (50 mm dia. graphite cathode of purity 99.999% and a retractable graphite anode rod of 7 mm dia. and purity 99.999%). The linear magnetic filter was energized using direct current (D.C.) power supply, and a magnetic field of ~350 G was achieved inside the duct. The chamber was initially pumped to a base pressure of ~10^{-6} mbar by the use of turbo molecular and rotary pump combination in the system, and then the high purity

(99.999%) helium gas was injected through the anode of 1 mm cavity at the cathode surface where arc was ignited. The a-C films were deposited on cleaned 7059 glass substrate and highly doped $\langle 100 \rangle n^{++}$ silicon substrates at a distance of ~35 cm away from the cathode, at a helium pressure of $\sim 8.6 \times 10^{-3}$ mbar. An additional negative substrate bias (direct current) ranging from 0 to −300 V was applied to the substrate at a fixed magnetic field of ~350 G to enhance the energy of the incoming ions. The negative terminal of the D.C. arc supply was connected to the cathode and the positive terminal to the anode striker rod. The body of the whole system was grounded and the duct was not biased. The films studied were deposited sequentially for 5 sec and then cooled for 50 sec. The process was repeated until the required thickness was obtained. The thickness of the film was in the range 200 ± 20 nm as measured by Talystep (Rank Taylor and Hobson) thickness profiler. The deposition rate achieved was in the range 6.0 ± 0.2 nm/sec.

2.2. Characterization of Samples. The phase analysis of the films was carried out by X-ray diffraction (Rigaku Miniflex II). The high-resolution transmission electron microscope (HRTEM) (Model FEI, Tecnai G2 F30-STWIN with field emission electron gun source) was operated at the electron accelerating voltage of 300 kV to explore the nano and subnanoscale structural information present in these films. For HRTEM samples, the a-C:nc films coated on silicon substrates were immersed in HF + HNO_3 mixtures which etched away Si substrates. On dilution of the mixtures with distilled water, the a-C:nc film floats on the surface of water. Subsequently, these self-supported films were lifted on a 200-mesh copper grid of 3.05 mm in diameter. The XPS measurements were carried out by (Perkin-Elmer model no. 1257) X-ray spectrophotometer operating at a base pressure of better than 6×10^{-10} mbar. From the dual anode X-ray source,

MgKα (1253.6 eV) line was used for the present analysis. The XPS wide scans were acquired using a 100 eV pass energy at a step of 1.0 eV, and XPS C1s core level spectra was acquired at 0.05 eV step with a pass energy of 60 eV. The spectra of the samples were recorded after sputter ion cleaning the top surface for 5 minutes by a differentially pumped argon ion gun. Unpolarized Raman spectra were recorded at room temperature using a Renishaw inVia Reflex micro-Raman spectrometer with a notch filter. Appropriate care was taken to avoid damaging the sample by laser excitation. The filtered radiation of 514.5 nm was used as the excitation source at a power of 15 mW. The spectra were scanned in the region 1100–1900 cm^{-1} with spectral resolution better than 1 cm^{-1} and a spatial resolution of about 1 μm. The residual stresses (S) in the films were evaluated (FSM Frontier Semiconductor (USA) instrument) using curvature method by using Stoney's equation [29]:

$$S = \frac{E t_s^2}{6(1-v)\, t_f}\left(\frac{1}{R} - \frac{1}{R_o}\right),\qquad(1)$$

where E and v are Young's modulus and Poisson's ratio of the substrate, respectively; t_s and t_f are the substrate thickness and the film thickness, respectively; R_o and R the radius of curvature of the substrate before and after film deposition. Values of $E/(1-v) \approx 180.5$ GPa have been used for silicon substrates. The radii of curvature R_o and R of the substrate and the films have been evaluated.

The nanomechanical properties of the films were measured using IBIS nanoindentation (Fisher-Cripps Laboratories Pvt. Ltd., Australia) using Berkovich indenter at maximum 1 mN load. Oliver and Pharr's [30] model is used to analyze the load versus displacement data. The field emission measurements were carried out using a parallel plate configuration using high voltage source meter (Keithley model 2410). An indium tin oxide-coated glass substrate was used as anode and a-C:nc films deposited on polished silicon substrates as cathode. The separation between the electrodes is defined by the pTFE spacer of thickness ∼50 μm, and the overlap area between the plate anode and cathode was kept at ∼0.196 cm^2. The current voltage (I-V) characteristic was measured at room temperature in a vacuum greater than 3×10^{-7} mbar maintained by a turbo-rotary-pump-based vacuum system. The emission current density (J) is calculated by dividing the emission current (I) by the area of the cathode, which is defined by the area of the hole in the spacer. The electric field (E) is obtained by voltage drop across the vacuum gap. Other experimental details are the same as published earlier [14, 28].

3. Results and Discussion

3.1. XRD of a-C:nc Films. Figure 2 shows the typical XRD pattern of a-C:nc film deposited at −60 V substrate bias with a fixed ∼350 G magnetic field. The broad peak at ∼26° shows the dominant amorphous nature of carbon film, and the reflection observed at ∼42.7° appears to be that of diamond (JCPDS file no. 791473). One more reflection is observed at 28.5° which is attributed to the silicon substrate (standard
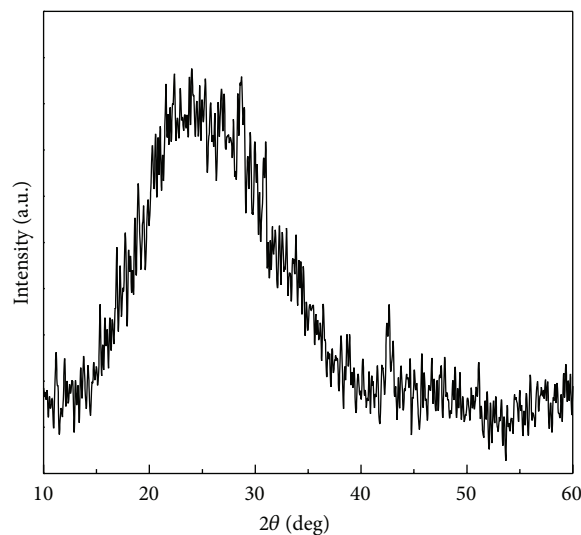

FIGURE 2: Typical X-ray diffraction patterns of a-C:nc film deposited at −60 V showing dominantly amorphous structure.

JCPDS file no. 772111). The peak at ∼42.7° along with the broad peak at 26° revealed the presence of nanocrystalline structure of carbon corresponding to diamond cubic which is dispersed in the amorphous carbon matrix. Other peaks related to diamond structure are absent may be due to the dominating amorphous nature present in the films. Similar patterns were observed in a-C:nc films deposited at other substrate biases. The crystalline size evaluated from the Scherer formula for the reflection observed at 42.7° is found to be ∼14 nm. This is found to be in agreement with the results reported in the literature [31].

3.2. HRTEM of a-C:nc Films. Figure 3 shows a set of HRTEM micrographs of a-C:nc film deposited at −60 V substrate bias which exhibit the distribution of nanocrystallites in the amorphous matrix. A uniform thin film microstructure with embedded crystalline nanoparticle has been discerned throughout the entire film (Figure 3(a)). In general, the crystalline zones are completely immersed in the amorphous matrix (Figure 3(b)). A grey contrast seen in the microstructure is evolved due to the presence of coexisting crystalline and amorphous forms of the carbon (Figure 3(a)). At high magnification in a particular region, one can see an aggregate of nanocrystallites in the film microstructure (marked with dotted circle in Figure 3(c)). The selected area electron diffraction pattern (SAEDP) recorded from the film microstructure showed a diffused ring pattern which confirms the presence of dominant amorphous structure (inset in Figure 3(c)). In another micrograph, coexisting nanocrystallites dispersed in the amorphous matrix elucidate the presence of nanocrystallites with good contrast which is normally evolved due to the overlap of tiny crystals along a particular crystallographic orientation (Figure 3(d)). Lattice scale images recorded from the coexisting crystalline nanoparticles with amorphous structure clearly reveal that the nanocrystallites are constituted of well-defined atomic
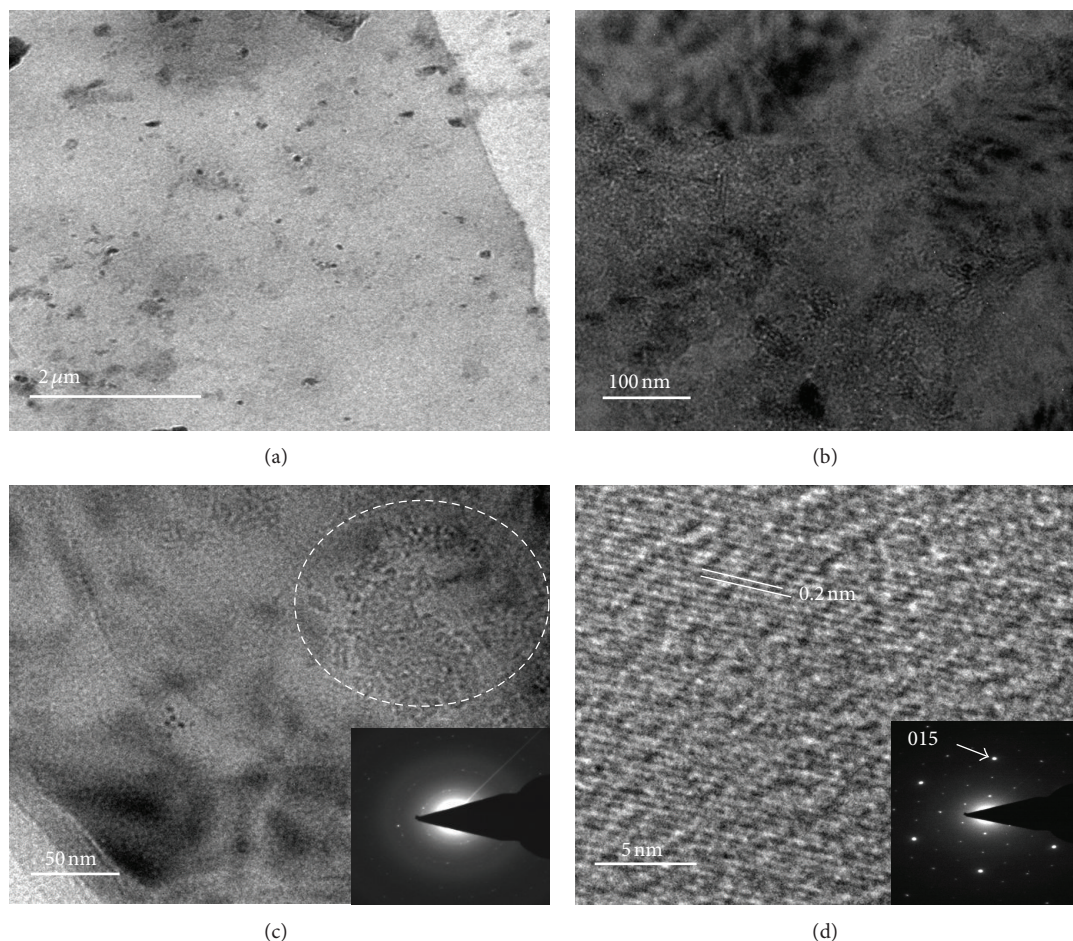
(a)

(b)

(c)

(d)

FIGURE 3: (a) to (d) HRTEM micrographs showing the distribution of ultrafine nanocrystallites of a-C:nc film deposited at −60 V substrate bias.

planes. The planes with d spacing of 0.2 nm (hkl 015) of diamond (rhombohedra, SGR$\bar{3}$m, a = 0.25221 and c = 4.3245 nm, JCPDS no. 79-1473) are marked on the micrograph (Figure 3(d)). However, the featureless contrast of amorphous structure has also been observed (Figure 3(d)). A SAEDP recorded from this region shows a single crystal spotty pattern with a sixfold axis of rhombohedra lattice which further corroborates with the single crystalline nature of the nanocrystallites (inset in Figure 3(d)). Ultrafine nanograined microstructures with average grain size between 20 and 30 nm are observed throughout the film with a majority of the grains of single crystallites. The grain size evaluated from the XRD pattern is found to be consistent with the grain size evaluated from the HRTEM study.

Gamaly and Ebbesen [18] suggested that nanoparticles can only be formed in the vicinity of target surface because carbon vapor is dense enough in this region for nanoparticles formation through the interaction of carbon atoms. Alexandrou et al. [23] deposited a-C thin film using anodic jet carbon arc technique and stated that the key element in forming continuous thin film instead of powder or soot in the carbon arc discharge process is to replace the high gas pressure in the whole chamber with a high gas pressure in the vicinity of the electric arc by introducing the gas in the

form of jet through an orifice in one of the two electrodes. In this way, the rest of the chamber is kept at low enough pressure for expanding plasma to reach the substrate. Carbon nanoparticle agglomerates are incorporated into the growing film. These carbon nanoparticles are first formed on the cathode surface with the right combination of local gas pressure and arc current density. Subsequent arc around the same spot delivers them with the carbon vapor to the substrate [23]. The presence of a magnetic field during the growth of the film in the present study might have facilitated the removal of neutrals and molten droplets from the carbon vapors reaching the substrate which in turn promotes nanocrystallite formation in the films deposited instead of fullerene and nanotubes. Zhang and Komvopoulos [32] have stabilized the plasma fluctuation and oriented the plasma flow in the cathodic vacuum arc system by applying magnetic field of the cathode coil which enabled the deposition of high-quality amorphous carbon films. This magnetic field provides a dual effect of maintaining dc arc current discharge and inhibits the migration of arc spots on the cathode surface.

3.3. XPS Measurements of a-C:nc Films.
The general XPS scan of the a-C:nc films showed only oxygen (O 1s~532 eV) as a surface contaminant in addition to the main peak of
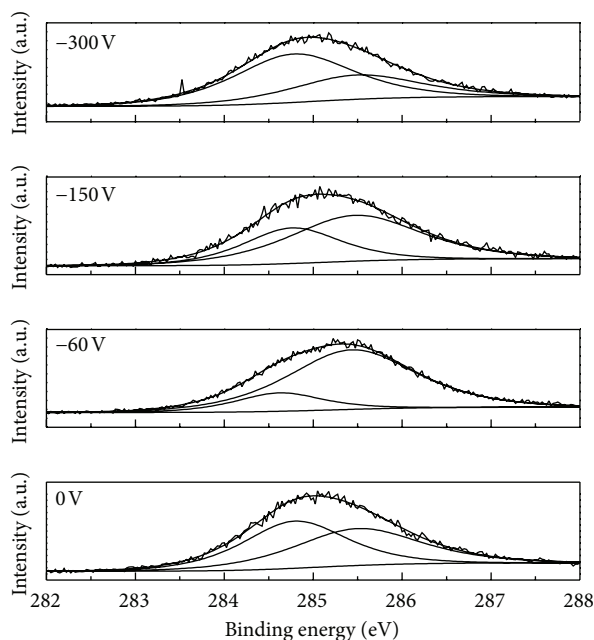
FIGURE 4: C1s peak position and deconvoluted spectra versus binding energy of a-C:nc films deposited at different negative substrate biases.

carbon (C1s ~ 285 eV) in all the a-C:nc films, and all other contaminant levels are below the XPS detection limit. The surface was cleaned by sputter etching using a rastered argon (Ar) ion beam at 4 keV, at a base pressure of ~10^{-8} mbar, for 5 min. The oxygen peak completely diminished after cleaning by argon ion bombardment in all the samples, indicating that the oxygen was present only on the surface and not throughout the bulk of the film. The oxygen content present in the films might have come from the laboratory exposure of the sample, and the bulk of the films were free from oxygen. Figure 4 shows the typical C1s spectra and deconvoluted spectra of a-C:nc films deposited at different negative substrate biases ranging from 0 to −300 V. It is evident from the figure that C1s peak occurs at 285.09 eV and its full width at half maximum (FWHM) value is 1.54 eV in a-C:nc film deposited at 0 V substrate bias. By applying substrate bias, the C1s peak shifted to the higher binding energy side up to −60 V, and after that it goes to the lower binding energy and occurs at 285.15 ± 0.10 eV in a-C:nc films deposited at −150 V and −300 V substrate biases. The FWHM of a-C:nc film deposited at −60 V substrate bias increased to 1.61 eV and to 1.59 eV in a-C:nc film deposited with −150 V substrate bias and to 1.62 eV in a-C:nc film deposited with −300 V substrate bias. Diaz et al. [33] were the first to evaluate the sp^3 content from the C1s peak of carbon by the deconvolution method which has been used to determine the sp^3 and sp^2 contents in a-C:nc films in the present investigation. For evaluating the bonding states, the C1s peak has been deconvoluted into two components of Lorentzian peaks after subtracting the background from the spectra by linear mode. The deconvoluted components were present at ~284.71 ± 0.08 and 285.46 ± 0.03 eV, and these were assigned to C=C sp^2 hybridized carbon in graphite-like carbon-carbon

bonds and sp^3 hybridized carbon in C-C in diamond-like structure, respectively. Thus, the area under these curves directly gives the amount of the sp^3 and sp^2 contents. The observed peak positions for deconvoluted component are well matched with the value reported in the literature [34, 35]. Figure 5 shows the variation of C1s, FWHM, sp^3, and sp^2 obtained in a-C:nc films versus negative substrate biases. The line has been drawn as a guide to the eye. It is evident from the figure that the sp^3 and sp^2 of a-C:nc film deposited at 0 V substrate bias are found to be 48.8 at. % and 51.2 at. %, respectively. The sp^3 is found to increase and sp^2 is found to decrease with the increase of substrate bias up to −60 V, and beyond −60 V substrate bias there is a reversal in the trend. We also observed a shift in the C1s peak towards higher binding energy up to −60 V. The determination of sp^3 content by analysis of XPS C1s peak in the a-C:nc film is much more straightforward method, and this also provided results which are representative of the bulk of the film than the method which uses the XAES C KLL peaks [14]. The method adopted in this study does not require any reference samples nor interpolation or differentiation, which is the case with latter technique, and it yields more accurate results since it does not have hydrogen or nitrogen in the film [36]. The value of sp^3 content (82.6 at. %) evaluated in a-C:nc films deposited at −60 V substrate bias in the present study is found to be larger than the value of sp^3 content (50 at. %) evaluated in a-C films having fullerene and nanotubes by Chhowalla et al. [20], larger than the value of sp^3 (73.8 at. %) evaluated in a-C:nc film deposited at −150 V substrate bias by FCJCA technique [28], and larger than the value of sp^3 (79.8 at.%) evaluated in ta-C film deposited at −200 V substrate bias by FCVA technique [14].

3.4. Raman Measurements of a-C:nc Films. The Raman spectra together with the deconvoluted spectra with the baseline drawn of a-C:nc films deposited at different negative substrate biases in the wave number range of 1100–1900 cm^{-1} are shown in Figures 6(a)–6(d). The a-C:nc films exhibit two bands: D (disorder) band at ~1406 ± 23 cm^{-1} and G (graphite) band at ~1565 ± 5 cm^{-1}. It is evident from the figure that all the spectra showed a broad peak at around 1560–1570 cm^{-1} and a discernible shoulder or hump at about 1380–1429 cm^{-1}. The a-C:nc film deposited at 0 V substrate bias shows some peak at 1350 cm^{-1}, and those films deposited at other substrate biases do not show such peak. The Raman spectra in all the samples appear to be symmetrical except the sample deposited at 0 V substrate bias. Further some sharp peak at about 1565 cm^{-1} may be due to the noise in the spectra. The deconvolution has been made in such a way that it looks similar in all the spectra. The degree of uncertainty in the fit varies from 2 to 3%. The values of G band peak position, G-FWHM, D band peak position, and D-FWHM and intensity ratio of D band to G band (I_D/I_G) obtained in a-C:nc films at different negative substrate biases have been summarized in Table 1. The a-C:nc film deposited at 0 V substrate bias showed G band at ~1570.1 cm^{-1} with G-FWHM of 112.42 cm^{-1} and a shoulder (D band) at ~1405.2 cm^{-1} with D-FWHM of 203.37 cm^{-1} accompanied with I_D/I_G = 0.57. The a-C:nc film deposited

TABLE 1: Parameters evaluated from Raman spectra in a-C:nc films deposited at different negative substrate biases.

Substrate bias/parameters	0 V	−60 V	−150 V	−300 V
G band (cm^{-1})	1570.1	1560.5	1560.0	1569.9
G-FWHM (cm^{-1})	112.4	176.3	172.2	149.8
D band (cm^{-1})	1405.2	1380.6	1428.3	1410.4
D-FWHM (cm^{-1})	203.4	178.4	229.0	257.4
I_D/I_G	0.6	0.3	0.5	0.8

up to −60 V substrate bias showed a shift in G and D bands to the lower wave number, decrease in I_D/I_G and D-FWHM, and increase of G-FWHM. Beyond −60 V substrate bias, there is a reversal in the trend where I_D/I_G, D-FWHM started increasing and G-FWHM started decreasing. It is well known that Raman scattering is a resonance process in which those configurations whose band gap match the excitation energy are preferentially excited. Visible Raman spectroscopy is 50–230 times [37, 38] more sensitive to sp^2 sites than sp^3 sites because visible photons (2.2 eV) preferentially excite the π states. Therefore, visible Raman spectroscopy is able to probe only the sp^2 sites. It depends fundamentally on the ordering of sp^2 sites and only indirectly on the fraction of sp^3 sites [39]. Therefore, the use of visible excitation source at 514.5 nm for the Raman measurements restricts the estimation of sp^3 fraction to indirect means like hump at around 1360–1450 cm^{-1} as D band and G peak, whose position shifts and the width indicates the relative concentration of sp^2 bonded carbon and the nature of carbon cluster in the film [1, 12, 40]. The band positions obtained in a-C:nc films are well matched with the band position observed by other group [39]. The deconvoluted Raman spectra show two Gaussian peaks after subtraction of the background from the spectra by linear method and are associated with their microstructures with the G band at around 1560–70 cm^{-1} due to symmetric E_{2g} C-C structure mode disordered graphite and D band at around 1380–1430 cm^{-1} presumably due to bond angle disorder in microdomains affected by sp^3 bonds of diamond. For the indirect qualitative evaluation of the amount of the sp^3 and sp^2 contents present in the films, the intensity ratio of the D band to G band (I_D/I_G) has been used [39]. The intensity ratio is found to decrease in a-C:nc films deposited up to −60 V substrate bias, and beyond −60 V substrate bias the trend is reversed. The same trend follows if we take the area of D and G bands, and thus care has been taken in evaluating I_D/I_G ratio. The decrease of I_D/I_G is related to the increase of sp^3 content, and this corroborates with the result evaluated from the XPS study which is found to be consistent with the study already reported [1, 39, 40]. Thus, with the application of substrate bias up to −60 V in a-C:nc films sp^3 content present in the film increases, and beyond −60 V substrate bias there is a reversal in the trend.

3.5. Mechanical Properties of a-C:nc Films. Load versus displacement curves of a-C:nc films deposited at different negative substrate biases of (a) 0 V, (b) −60 V, (c) −150 V, and (d) −300 V are shown in Figure 7. The arrow shows the
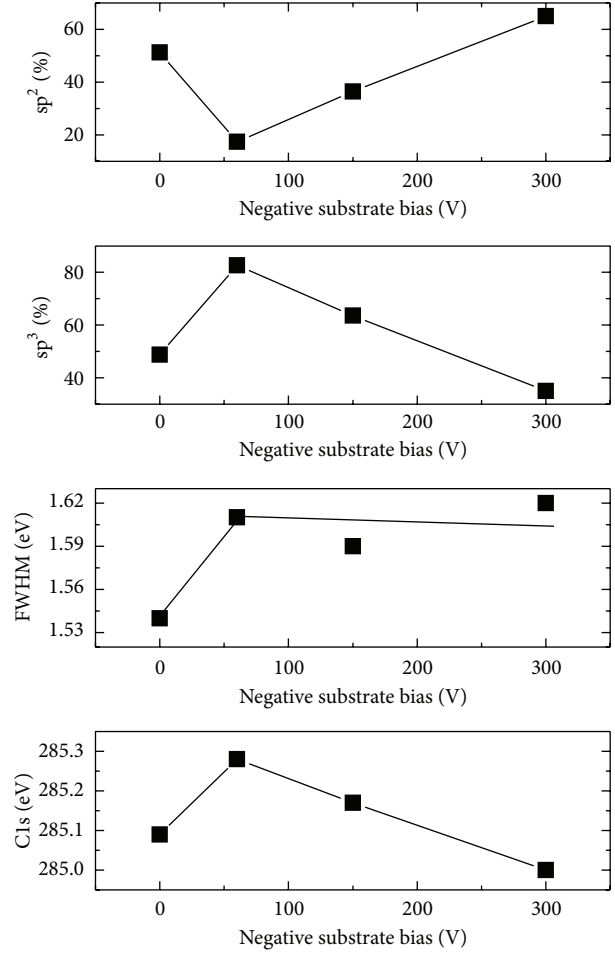

FIGURE 5: Variation of C1s, FWHM, sp^3, and sp^2 evaluated in a-C:nc films versus negative substrate biases.

direction of loading and unloading curves, and the initial starting load is 0.15 mN in all the curves. The penetration depths of a-C:nc films were varied in the range of 25–32 nm. The residual stresses (S) present in a-C:nc films are found to be compressive in nature, and the values lie in the range of 1.90–9.68 GPa. The variation of hardness (H), elastic modulus (E), plastic index parameter (H/E), and percentage elastic recovery (%ER) evaluated in the a-C:nc films versus negative substrate biases is shown in Figure 8. We have drawn a line as a guide to the eye. The values of H, E, H/E, and %ER of a-C:nc films deposited at 0 V substrate bias are found to be 41.0 GPa, 328.6 GPa, 0.125, and 84.3, respectively. It is evident from the figure that the values of H, E, H/E, and %ER evaluated in the a-C:nc films first increase up to −60 V substrate bias, and beyond −60 V substrate bias there is a reversal in the trend and the values of these parameters are found to decrease. a-C:nc film deposited at −60 V substrate bias in the present study showed the values of H ~ 58.3 GPa, E ~ 426.2 GPa, H/E ~ 0.136, and %ER ~ 86.3, respectively. Many groups [41, 42] have systematically studied the effect of substrate bias on the mechanical properties of thin films. They have considered two different cases of hard film on soft substrate and soft film on hard substrate.
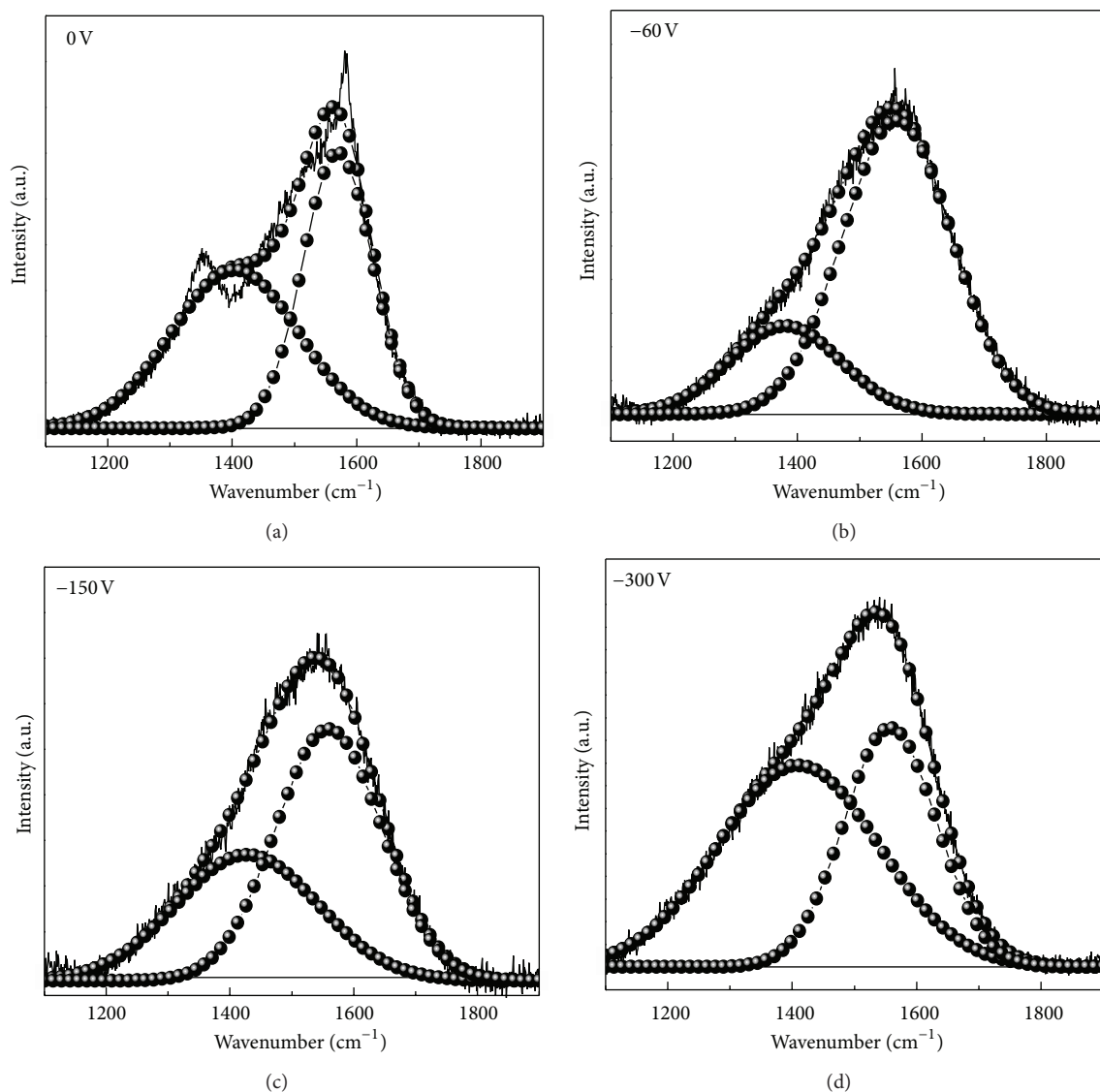
Figure 6: (a) to (d) Raman spectra and deconvoluted spectra of a-C:nc films deposited at different negative substrate biases in the wave number range of 1100–1900 cm^{-1}.

They have realized that hard film on soft substrate exhibited increase in hardness with the increase in penetration depth. In the present study, reported value of hardness may be the composite hardness of the film and substrate [43]. The hardness values of a-C:nc films in the present study are found to be larger than the hardness value of silicon substrate which belongs to the former case discussed. Mostly nanomechanical characterization should be performed within 10% of the film thickness. In the present study, the indentation depths in all the a-C:nc films have crossed the limit. It may be due to the effect of soft silicon substrate. The value of hardness reported in the present study might be a lower value whereas the actual value of hardness may be larger than the reported value [43]. The compressive residual stress present in a-C films is found to follow the trend of hardness and elastic modulus, and it is revealed from the reported literature that the residual stress and hardness of the films have similar type of behavior with the increase of negative substrate bias [44]. The hardness values of the a-C:nc films are found to depend strongly on the sp^3 content. Elastic modulus of films shows the amount of deformation under applying external force. Elastic recovery can provide the elastic information as penetration depth. In the present work, elastic recovery is found to vary linearly with sp^3 content of a-C:nc films. The plastic index parameter (H/E) [45] is an important parameter to differentiate between the elastic and elastic-plastic behaviors. For protective coating over a magnetic hard disc or good wear-resistant coating over that, H/E ratio must be very high. This is the reason why less hard films having high H/E ratio is widely accepted for this kind of applications. The H/E ratio is used to describe the deformation mechanism of the material. High value of H/E means that these films are highly resistant to plastic deformation. It may be worth to note that the values of H/E reported here are larger than
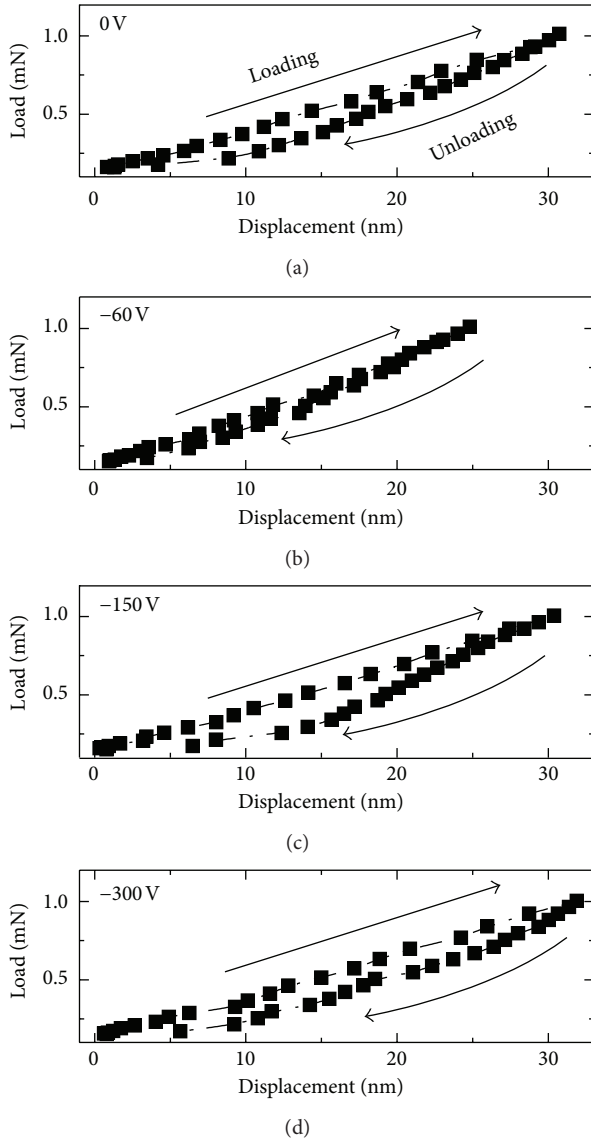
(a)

(b)

(c)

(d)

FIGURE 7: Load-displacement curves of a-C:nc films deposited at different negative substrate biases of (a) 0 V, (b) −60 V, (c) −150 V, and (d) −300 V.

FIGURE 8: Variation of H, E, H/E, and %ER of a-C:nc films versus negative substrate biases.

those reported for ta-C films (0.10–0.12) by other workers [45]. Neuville and Matthews [40] have provided a coherent perspective on the many factors which are important for optimization and appropriate use of hard coatings while also challenging certain preconditions. Charitidis [45] while studying the nanomechanical and tribological properties of carbon-based thin films stated that the hardness and elastic modulus of a-C films depend upon their local bonding and mean coordination of network. The elastic recovery of carbon based thin film was related to its density and hybridization. The effect of gaseous environment of amorphous carbon thin films having embedded nanocrystallites deposited by filtered cathodic jet carbon arc (FCJCA) technique at −300 V substrate bias has been studied by us [46], where the sp^3 content and hardness values were found to increase with the change of gaseous environment from helium to nitrogen to
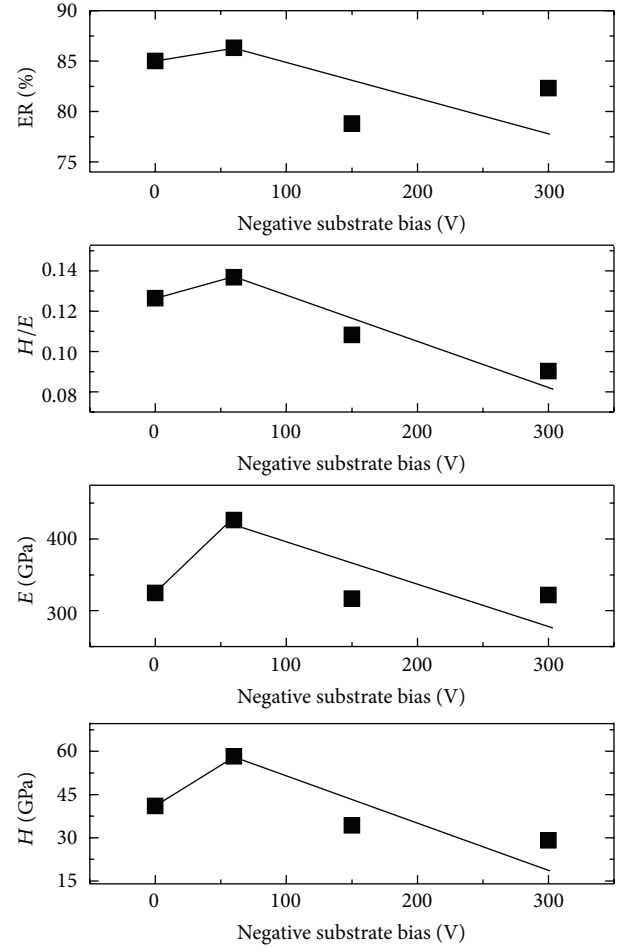
without gas and to hydrogen. The values of nanomechanical properties obtained in a-C films deposited at −60 V substrate bias by FAJCA technique in the present study are found to be consistent with those of a-C films using similar method by Chhowalla et al. [20] and with those of a-C films having embedded nanocrystallites deposited by FCJCA technique at the same bias [28]. Thus, a-C:nc films are significantly harder than the ta-C films deposited by S bend FCVA process [15].

3.6. Field Emission Properties of a-C:nc Films. Figure 9 shows the variation in field emission current density (J) versus electric field (E) characteristics of a-C:nc films deposited at different negative substrate biases. Field emission involves a quantum-mechanical process in which electrons tunnel out of the electrodes into vacuum when subjected to a very high electric field. It is a nonlinear process, in which the J-E characteristics are usually described by the classical Fowler and Nordheim (FN) equation [47, 48]:

$$J = A \left[\frac{(\beta E)^2}{\varphi} \right] \exp \left(-\frac{B\varphi^{3/2}}{\beta E} \right), \tag{2}$$

where J is the current density, φ is the potential barrier height (taken as the work function), E is the applied electric field, β is the field enhancement factor, and a and b are constants and have the values of 1.54×10^{-6} AV^{-2} and 6.83×10^9 V/meV$^{2/3}$, respectively. The plots of log (J/E^2) versus $1/E$ for the corresponding J-E characteristics are shown in inset of Figure 9. These plots are straight lines which confirm that the J-E characteristics follow the FN relation. The threshold field of emission (E_T) is defined as the applied electric field at which an emission current density of $\sim 1 \times 10^{-6}$ A/cm^2 is obtained and is shown by the arrow in each curve. The slopes of these plots give the effective emission barriers φ, if we assume an ideal plane emitter with a field enhancement factor β of 1. The values of φ for a-C:nc films grown were in the range of 0.064–0.124 eV. Other worker [49] reported similar values of $\varphi = 0.04$–0.1 eV. These values are obviously quite low, and the true barrier may be much larger [10]. If we take a work function (φ) of 5 eV, typical of graphite bonding, then the FN slopes correspond to the field enhancement factor β of 254.8–694.4 for these a-C:nc films. We understand that β, in the case of a parallel-plate arrangement and flat cathodes, is not a realistic estimation because emission is from discrete points. However, we wanted to see whether the estimated parameters, even though not accurate, correlates to some other calculated value or shows a consistent trend with a change in material properties with a change in process parameters. The values of E_T, J_{max} at 20 V/μm, slope m of FN plots, φ, and β of a-C:nc films grown at different negative substrate bias are summarized in Table 2. The values of E_T of 9.4–14.1 accompanied with J_{max} 0.04–0.6 mA/cm^2 in a-C:nc films deposited at different negative substrate biases are found to be consistent with the values of E_T and J_{max} obtained in ta-C films deposited using an L bend FCVA system at ion energy of 80–100 V as reported by Satyanarayana et al. [49]. These values are also consistent with the values of ta-C films deposited using S bend FCVA system at substrate biases of -150 V to -200 V [50]. For good field emission, optimum values of sp^3 and sp^2 bonding are needed. Carey et al. [51] had shown in their study that defect and localized states near Fermi level help to obtain efficient field emission with $E_T < 10$ V/μm. Although many research groups [52, 53] reported low E_T and large J_{max} in carbon nanotubes (CNTs) and carbon nanowalls grown by many complex and expensive techniques, there are many technological problems in the fabrication of large area field emission devices with these CNTs. These a-C:nc films deposited by FAJCA technique with enhanced nanomechanical and field emission properties seem to be very encouraging.

4. Conclusions

The effect of negative substrate bias on the structural, nanomechanical, and field emission properties of a-C:nc films deposited by FAJCA technique has been studied. HRTEM investigation revealed an amorphous structure with nanocrystallites of size 20 to 30 nm embedded in the amorphous matrix. The values of sp^3, H, E, H/E, and %ER are found to increase and those of sp^2 and I_D/I_G ratio are found
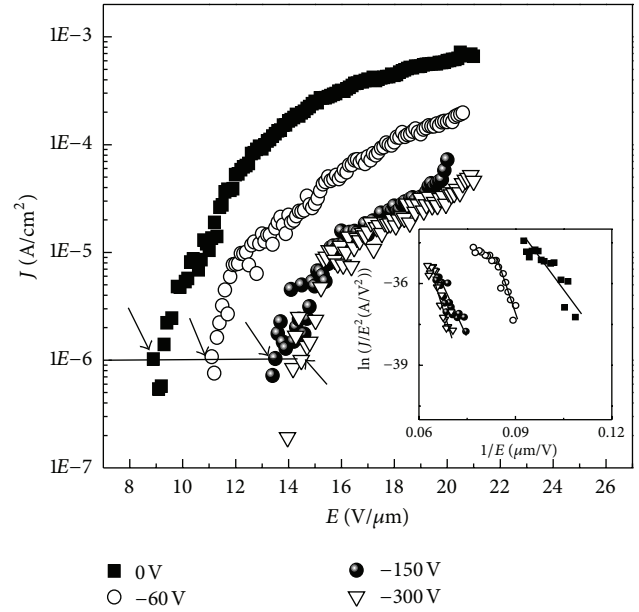

FIGURE 9: Field emission characteristics of the a-C:nc films deposited at different negative substrate biases. Inset shows their FN plots.

TABLE 2: Emission parameters evaluated in a-C:nc films deposited at different negative substrate biases.

Substrate bias/properties	0 V	−60 V	−150 V	−300 V
E_T (V/μm)	9.4	11.0	13.5	14.1
J_{max} (mA/cm^2) at 20 V/μm	0.6	0.2	0.07	0.04
Slope m of FN plots (V/μm)	109.9	161.2	166.1	299.7
φ (eV) (at $\beta = 1$)	0.064	0.084	0.082	0.124
β (for $\varphi = 5$ eV)	694.4	473.7	459.8	254.8

to decrease with the increase of substrate bias up to -60 V, and beyond -60 V substrate bias there is a reversal in trend of these parameters. However, the values of J_{max} and β were found to decrease and that of E_T increased continuously with the increase of substrate bias up to -300 V. Maximum hardness of 58.3 GPa accompanied with $E = 426.2$ GPa, $H/E = 0.136\%$, %ER = 86.3, and sp^3 = 82.6% has been obtained in a-C:nc film deposited at -60 V substrate. The a-C:nc films deposited by FAJCA technique may have the potential to be a thin film equivalent to carbon nanotubes in terms of mechanical and field emission properties.

Research Highlight

(i) a-C films with embedded nanocrystallites are grown by filtered anodic jet carbon arc technique.

(ii) HRTEM reveals the embedded nanocrystallites in amorphous matrix of the a-C:nc film.

(iii) The properties of a-C:nc films depend on negative substrate bias.

(iv) Enhanced hardness and field emission have been observed.

Acknowledgments

References

[1] J. Robertson, "Diamond-like amorphous carbon," *Materials Science and Engineering R*, vol. 37, no. 4–6, pp. 129–281, 2002.

[2] S. R. P. Silva, G. A. J. Amaratunga, and C. P. Constantinou, "Optical properties of amorphous C/diamond thin films," *Journal of Applied Physics*, vol. 72, no. 3, pp. 1149–1153, 1992.

[3] J. Robertson, "Plasma deposition of diamond-like carbon," *Japanese Journal of Applied Physics*, vol. 50, Article ID 01AF01, 8 pages, 2011.

[4] D. S. da Silva, A. D. S. Côrtes, M. H. Oliveira Jr. et al., "Application of amorphous carbon based materials as antireflective coatings on crystalline silicon solar cells," *Journal of Applied Physics*, vol. 110, no. 4, Article ID 043510, 2011.

[5] M. Umeno and S. Adhikary, "Diamond-like carbon thin films by microwave surface-wave plasma CVD aimed for the application of photovoltaic solar cells," *Diamond and Related Materials*, vol. 14, no. 11-12, pp. 1973–1979, 2005.

[6] W. S. Choi, K. Kim, J. Yi, and B. Hong, "Diamond-like carbon protective anti-reflection coating for Si solar cell," *Materials Letters*, vol. 62, no. 4-5, pp. 577–580, 2008.

[7] S. K. Das, M. Patel, and A. J. Bhattacharyya, "Effect of nanostructuring and ex situ amorphous carbon coverage on the lithium storage and insertion kinetics in anatase titania," *ACS Applied Materials & Interfaces*, vol. 2, no. 7, pp. 2091–2099, 2010.

[8] S. Salvatori, G. Mazzeo, G. Conte, M. C. Rossi, and V. Ralchenko, "Polycrystalline diamond position sensitive detector for excimer laser UV radiation," *Diamond and Related Materials*, vol. 13, no. 4–8, pp. 948–953, 2004.

[9] N. S. Xu and S. E. Huq, "Novel cold cathode materials and applications," *Materials Science and Engineering R*, vol. 48, no. 2–5, pp. 47–189, 2005.

[10] O. S. Panwar, N. L. Rupesinghe, and G. A. J. Amaratunga, "Field emission from as grown and nitrogen incorporated tetrahedral amorphous carbon/silicon heterojunctions grown using a pulsed filtered cathodic vacuum arc technique," *Journal of Vacuum Science and Technology B*, vol. 26, no. 2, pp. 566–575, 2008.

[11] X. Xiao, J. Partridge, M. Taylor, and D. McCulloch, "The stress and microstructure of a-C multilayers deposited using a filtered cathodic vacuum arc and periodic substrate bias," *Physica Status Solidi (C)*, vol. 6, no. 10, pp. 2179–2183, 2009.

[12] P. J. Fallon, V. S. Veerasamy, C. A. Davis et al., "Properties of filtered-ion-beam-deposited diamondlike carbon as a function of ion energy," *Physical Review B*, vol. 48, no. 7, pp. 4777–4782, 1993.

[13] E. Rismani, S. K. Sinha, H. Yang, and C. S. Bhatia, "Effect of pretreatment of Si interlayer by energetic C+ ions on the improved nanotribological properties of magnetic head

overcoat," *Journal of Applied Physics*, vol. 111, no. 8, Article ID 084902, 10 pages, 2012.

[14] O. S. Panwar, M. A. Khan, M. Kumar et al., "Effect of high substrate bias and hydrogen and nitrogen incorporation on filtered cathodic vacuum arc deposited tetrahedral amorphous carbon films," *Thin Solid Films*, vol. 516, no. 8, pp. 2331–2340, 2008.

[15] O. S. Panwar, M. A. Khan, G. Bhagavanarayana, P. N. Dixit, S. Kumar, and C. M. S. Rauthan, "Effect of hydrogen and nitrogen incorporation on the properties of tetrahedral amorphous carbon films grown using S bend filtered cathodic vacuum arc process," *Indian Journal of Pure and Applied Physics*, vol. 46, no. 11, pp. 797–805, 2008.

[16] P. Tian, X. Zhang, and Q. Z. Xue, "Enhanced room-temperature positive magnetoresistance of a-C:Fe film," *Carbon*, vol. 45, no. 9, pp. 1764–1768, 2007.

[17] D. Wan and K. Komvopoulos, "Tetrahedral and trigonal carbon atom hybridization in thin amorphous carbon films synthesized by radio-frequency sputtering," *Journal of Physical Chemistry C*, vol. 111, no. 27, pp. 9891–9896, 2007.

[18] E. G. Gamaly and T. W. Ebbesen, "Mechanism of carbon nanotube formation in the arc discharge," *Physical Review B*, vol. 52, no. 3, pp. 2083–2089, 1995.

[19] G. A. J. Amaratunga, M. Chhowalla, C. J. Kiely, I. Alexandrou, R. Aharonov, and R. M. Devenish, "Hard elastic carbon thin films from linking of carbon nanoparticles," *Nature*, vol. 383, no. 6598, pp. 321–223, 1996.

[20] M. Chhowalla, R. A. Aharonov, C. J. Kiely, I. Alexandrou, and G. A. J. Amaratunga, "Generation and deposition of fullerene- and nanotube-rich carbon thin films," *Philosophical Magazine Letters*, vol. 75, no. 5, pp. 329–335, 1997.

[21] I. Alexandrou, H.-J. Scheibe, C. J. Kiely, A. J. Papworth, G. A. J. Amaratunga, and B. Schultrich, "Carbon films with an sp^2 network structure," *Physical Review B*, vol. 60, no. 15, pp. 10903–10907, 1999.

[22] I. Alexandrou, M. Baxendale, N. L. Rupesinghe, G. A. J. Amaratunga, and C. J. Kiely, "Field emission properties of nanocomposite carbon nitride films," *Journal of Vacuum Science and Technology B*, vol. 18, no. 6, pp. 2698–2703, 2000.

[23] I. Alexandrou, C. J. Kiely, A. J. Papworth, and G. A. J. Amaratunga, "Formation and subsequent inclusion of fullerene-like nanoparticles in nanocomposite carbon thin films," *Carbon*, vol. 42, no. 8-9, pp. 1651–1656, 2004.

[24] P. K. Chu and L. Li, "Characterization of amorphous and nanocrystalline carbon films," *Materials Chemistry and Physics*, vol. 96, no. 2-3, pp. 253–277, 2006.

[25] C. Biswas and Y. H. Lee, "Graphene versus carbon nanotubes in electronic devices," *Advanced Functional Materials*, vol. 21, no. 20, pp. 3806–3826, 2011.

[26] D. Varshney, C. V. Rao, M. J.-F. Guinel, Y. Ishikawa, B. R. Weiner, and G. Morell, "Free standing graphene-diamond hybrid films and their electron emission properties," *Journal of Applied Physics*, vol. 110, no. 4, Article ID 044324, 2011.

[27] C. P. Lungu, C. E. A. Grigorescu, M. I. Rusu et al., "Nanodiamond crystallites embedded in carbon films prepared by thermionic vacuum arc method," *Diamond and Related Materials*, vol. 20, no. 7, pp. 1061–1064, 2011.

[28] Ishpal, O. S. Panwar, A. K. Srivastava et al., "Effect of substrate bias in amorphous carbon films having embedded nanocrystallites," *Surface and Coatings Technology*, vol. 206, no. 1, pp. 155–164, 2011.

[29] G. G. Stoney, "The tension of metallic films deposited by electrolysis," *Proceedings of the Royal Society A*, vol. 82, no. 553, pp. 172–175, 1909.

[30] W. C. Oliver and G. M. Pharr, "An improved technique for determining hardness and elastic modulus using load and displacement sensing indentation experiments," *Journal of Materials Research*, vol. 7, no. 6, pp. 1564–1583, 1992.

[31] P. D. Ownby, X. Yang, and J. Liu, "Calculated X-ray diffraction data for diamond polytypes," *Journal of the American Ceramic Society*, vol. 75, no. 7, pp. 1876–1883, 1992.

[32] H. S. Zhang and K. Komvopoulos, "Direct-current cathodic vacuum arc system with magnetic-field mechanism for plasma stabilization," *Review of Scientific Instruments*, vol. 79, Article ID 073905, 7 pages, 2008.

[33] J. Diaz, G. Paolielli, S. Ferrer, and F. Comin, "Separation of the sp^3 and sp^2 components in the C1s photoemission spectra of amorphous carbon films," *Physical Review B*, vol. 54, no. 11, pp. 8064–8069, 1996.

[34] G. G. Wang, H. Y. Zhang, H. F. Zhou et al., "Effect of ECR-assisted microwave plasma nitriding treatment on the microstructure characteristics of FCVA deposited ultra-thin ta-C films for high-density magnetic storage applications," *Applied Surface Science*, vol. 256, no. 10, pp. 3024–3030, 2010.

[35] R. McCann, S. S. Roy, P. Papakonstantinou, M. F. Bain, H. S. Gamble, and J. A. McLaughlin, "Chemical bonding modifications of tetrahedral amorphous carbon and nitrogenated tetrahedral amorphous carbon films induced by rapid thermal annealing," *Thin Solid Films*, vol. 482, no. 1-2, pp. 34–40, 2005.

[36] Ishpal, O. S. Panwar, M. Kumar, and S. Kumar, "X-ray photoelectron spectroscopic study of nitrogen incorporated amorphous carbon films embedded with nanoparticles," *Applied Surface Science*, vol. 256, no. 24, pp. 7371–7376, 2010.

[37] N. Wada, P. J. Gaczi, and S. A. Solin, "'Diamond-like' 3-fold coordinated amorphous carbon," *Journal of Non-Crystalline Solids*, vol. 35-36, no. 1, pp. 543–548, 1980.

[38] S. R. Salis, D. J. Gardiner, M. Bowden, J. Savage, and D. Rodway, "Monitoring the quality of diamond films using Raman spectra excited at 514.5 nm and 633 nm," *Diamond and Related Materials*, vol. 5, no. 6–8, pp. 589–591, 1996.

[39] A. C. Ferrari and J. Robertson, "Interpretation of Raman spectra of disordered and amorphous carbon," *Physical Review B*, vol. 61, no. 20, pp. 14095–14107, 2000.

[40] S. Neuville and A. Matthews, "A perspective on the optimisation of hard carbon and related coatings for engineering applications," *Thin Solid Films*, vol. 515, no. 17, pp. 6619–6653, 2007.

[41] R. Saha and W. D. Nix, "Effects of the substrate on the determination of thin film mechanical properties by nanoindentation," *Acta Materialia*, vol. 50, no. 1, pp. 23–38, 2002.

[42] X. Chen and J. J. Vlassak, "Numerical study on the measurement of thin film mechanical properties by means of nanoindentation," *Journal of Materials Research*, vol. 16, no. 10, pp. 2974–2982, 2001.

[43] B. Jönsson and S. Hogmark, "Hardness measurements of thin films," *Thin Solid Films*, vol. 114, no. 3, pp. 257–269, 1984.

[44] G. Capote, R. Piroli, P. M. Jardin, A. R. Zanatta, L. G. Jacobsohn, and F. L. Freirer Jr., "Amorphous hydrogenated carbon films deposited by PECVD: influence of the substrate temperature on film growth and microstructure," *Journal of Non-Crystalline Solids*, vol. 338–340, pp. 503–508, 2004.

[45] C. A. Charitidis, "Nanomechanical and nanotribological properties of carbon-based thin films: a review," *International Journal of Refractory Metals and Hard Materials*, vol. 28, no. 1, pp. 51–70, 2010.

[46] Ishpal, O. S. Panwar, M. Kumar, and S. Kumar, "Effect of ambient gaseous environment on the properties of amorphous carbon thin films," *Materials Chemistry and Physics*, vol. 125, no. 3, pp. 558–567, 2011.

[47] J. D. Carey, "Engineering the next generation of large-area displays: prospects and pitfalls," *Philosophical Transactions of the Royal Society A*, vol. 361, no. 1813, pp. 2891–2907, 2003.

[48] R. H. Fowler and L. Nordheim, "Electron emission in intense electric fields," *Proceedings of the Royal Society A*, vol. 119, no. 781, pp. 173–181, 1928.

[49] B. S. Satyanarayana, A. Hart, W. I. Milne, and J. Robertson, "Field emission from tetrahedral amorphous carbon," *Applied Physics Letters*, vol. 71, no. 10, pp. 1430–1432, 1997.

[50] O. S. Panwar, M. A. Khan, B. S. Satyanarayana et al., "Effect of high substrate bias and hydrogen and nitrogen incorporation on density of states and field-emission threshold in tetrahedral amorphous carbon films," *Journal of Vacuum Science and Technology B*, vol. 28, no. 2, pp. 411–422, 2010.

[51] J. D. Carey, R. D. Forrest, and S. R. P. Silva, "Origin of electric field enhancement in field emission from amorphous carbon thin films," *Applied Physics Letters*, vol. 78, no. 16, p. 2339, 2001.

[52] S. Talapatra, S. Kar, S. K. Pal et al., "Direct growth of aligned carbon nanotubes on bulk metals," *Nature Nanotechnology*, vol. 1, no. 2, pp. 112–116, 2006.

[53] S. Shimada, K. Teii, and M. Nakashima, "Low threshold field emission from nitrogen-incorporated carbon nanowalls," *Diamond and Related Materials*, vol. 19, no. 7–9, pp. 956–959, 2010.